mnIronNWA468.doc 10-Jun-02

A IAB-complex iron meteorite containing low-Ca clinopyroxene: Northwest Africa 468 and its relationship to lodranites and formation by impact melting

Alan E. Rubin[1], Gregory W. Kallemeyn[1] and John T. Wasson[1,2]

[1]Institute of Geophysics and Planetary Physics

University of California, Los Angeles, CA 90095-1567

[2]Also Departments of Earth and Space Sciences and Chemistry and Biochemistry

Abstract. Northwest Africa 468 (NWA 468) is a new ungrouped, silicate-rich member of the IAB complex of nonmagmatic iron meteorites. The silicates contain relatively coarse (~300 μm-size) grains of low-Ca clinopyroxene with polysynthetic twinning and inclined extinction. Low-Ca clinopyroxene is indicative of quenching from high temperatures (either from protoenstatite in a few seconds or high-temperature clinoenstatite in a few hours). It seems likely that NWA 468 formed by impact melting followed by rapid cooling to ≤660°C. After the loss of a metal-sulfide melt from the silicates, sulfide was reintroduced, either from impact-mobilized FeS or as an S_2 vapor that combined with metallic Fe to produce FeS. The O-isotopic composition ($\Delta^{17}O = -1.39‰$) indicates that the precursor material of NWA 468 was a metal-rich (e.g., CR) carbonaceous chondrite. Lodranites are similar in bulk chemical and O-isotopic composition to the silicates in NWA 468; the MAC 88177 lodranite (which also contains low-Ca clinopyroxene) is close in bulk chemical composition. Both NWA 468 and MAC 88177 have relatively low abundances of REE and plagiophile elements. Siderophiles in the metal-rich areas of NWA 468 are similar to those in the MAC 88177 whole rock; both samples contain low Ir and relatively high Fe, Cu and Se. Most unweathered lodranites contain ~20-38 wt.% metallic Fe-Ni. These rocks may have formed in an analogous manner to NWA 468 (i.e., by impact melting of metal-rich carbonaceous-chondrite precursors) but with less separation of metal-rich melts from silicates.

1. INTRODUCTION

Iron meteorite groups can be divided into magmatic and nonmagmatic categories. The largest set of nonmagmatic irons consists of members of the IAB complex (Wasson and Kallemeyn, 2002). Metal compositions in magmatic irons show very large ranges in Ir and other refractory siderophiles. For example, in groups IIAB and IIIAB, Ir ranges by factors of 5000 and 2000, respectively. Such large ranges can only be produced by fractional crystallization (resulting from slow cooling of continuously mixing magmas). The ranges in Ir are much smaller (factors <5) in the metal of irons from nonmagmatic groups; most of the compositional variations observed among these samples were not produced by fractional crystallization.

The largest nonmagmatic group is IAB. Wasson and Kallemeyn (2002) reexamined the properties of >160 irons including the irons earlier classified IAB and IIICD and a large set of ungrouped irons with similar compositions. They found that most IAB irons form a moderately tight cluster (which they called the main group) on element-element diagrams. In addition to the main group, there are three closely related low-Au subgroups and two more distantly related high-Au subgroups. The entire set (main group, subgroups and closely related ungrouped irons) was designated the IAB complex.

A large fraction of the IAB-complex irons contains silicates and C (occurring as graphite and/or carbides). In most of these meteorites, the proportion of silicates is small; most silicates are associated with FeS. Silicates can occur as rare coarse (>2 mm) clusters of grains and as abundant fine (<100 μm) grains. Coarse silicate inclusions were recently described by Benedix et al. (2000); these typically have chondritic mineralogy (olivine, low-Ca pyroxene, plagioclase, metal, troilite) as well as bulk chemical compositions that are approximately chondritic (Kracher, 1974; Bild, 1977; Benedix et al., 2000). The oxygen-isotopic compositions of these silicates are in the carbonaceous-chondrite range ($\Delta^{17}O < -0.3‰$ where $\Delta^{17}O = \delta^{17}O - 0.52\ \delta^{18}O$). Rare-gas abundances and rare-earth-element patterns of these silicate inclusions are also generally chondritic.

Wasson et al. (1980) and Choi et al. (1995) proposed that the IAB-complex irons formed as impact melts within the (mega) regoliths of chondritic asteroids. Benedix et al. (2000) modeled the IAB irons as products of a complex process involving partial melting (resulting from an internal heat source, probably ^{26}Al), incomplete differentiation, and metamorphism, followed by impact mixing. Wasson and Kallemeyn (2002) inferred that the high-temperature history of the IAB complex involved rapid heating and cooling, more consistent with impact heating than with radiogenic heating. In order to help evaluate such models we have studied NWA 468, a new member of the IAB complex that contains massive silicate inclusions. This 6100-g iron was obtained from a dealer in Alnif, Morocco before January 2000 (Grossman and Zipfel, 2001). The date of find is unknown.

2. ANALYTICAL PROCEDURES

The instrumental-neutron-activation-analysis (INAA) procedure of the metal was described by Wasson et al. (1989). Duplicate metal samples were cut to 3.1±0.2 mm thicknesses and to masses of 550±100 mg; surfaces were cleaned with SiC paper. After irradiation for 3 h with a neutron flux of $\sim 1.8\times10^{12}$ n cm^{-2} s^{-1} in the lazy susan of the Triga nuclear reactor at the University of California, Irvine, the samples were cleaned by a light etch and mounted onto cards for counting. Standards were the IIAB hexahedrites Filomena and Coahuila, and NBS standard steel 809B. Samples were counted four times over a period of four weeks. Well-defined gamma-ray peaks were integrated by algorithms in the SPECTRA program of Baedecker and Grossman (1989). Poorly defined peaks were plotted and integrated individually. Elemental precisions are given in Wasson and Kallemeyn (2002).

Neutron-activation of the silicate portion of NWA 468 was also performed at the University of California, Irvine reactor. Samples were irradiated for 4 h and counted several times over a period of ~6 weeks to determine Na, K, Ca, Sc, Cr, Mn, Fe, Co, Ni, Zn, Ga, As, Se, Sb, REE, Os, Ir and Au. Samples were later irradiated for 2 min and counted immediately to determine Mg, Al, V and Ca. Relative standard deviations can be found in Kallemeyn et al. (1989).

The oxygen-isotopic compositions were determined at the University of Chicago using BrF_5 extraction and mass-spectrometric analysis of the evolved O_2 (Clayton and Mayeda, 1963; Clayton et al., 1976).

A 62-g sample of NWA 468 from the UCLA meteorite collection (LC 1706) and additional polished thin sections were studied microscopically in transmitted and reflected light. Grain sizes were determined microscopically using a calibrated reticle. Lodranite thin section MAC 88177,16 was also studied microscopically. Mineral analyses of NWA 468 were made with the Cameca Camebax electron

microprobe at UCLA using natural and synthetic standards, 20-s counting times, and PAP corrections (the Cameca version of ZAF corrections). Modal analyses of opaque phases and of low-Ca clinopyroxene and orthopyroxene were made with a petrographic microscope using an automated point counter; modal analyses of silicate phases in NWA 468 were determined by EDS with the Cameca microprobe. These modes were combined.

3. RESULTS

3.1 Bulk Composition of the Metal

The composition of the metal portion of NWA 468 is listed in Table 1; the position of this meteorite relative to the ~160 irons in the IAB complex (Wasson and Kallemeyn, 2002) is shown in Fig. 1. The dominant cluster of dark diamonds on the left side of the diagram are the 70 members of the IAB main group (MG). There are five subgroups with 6 to 15 members each that are assigned letters based on their Au contents (L = low, ≤2.0 µg/g Au, H = high, ≥2.1 µg/g Au) and their Ni contents (H = high, >170 mg/g Ni; M = medium, ~110-145 mg/g Ni; L = low, ~75-90 mg/g Ni). Thus, the dark-filled circles plotting appreciably above the main group in Fig. 1a are subgroup sLH (low Au, high Ni). Most members of this subgroup were originally designated group IIID by Wasson and Schaudy (1971). More details about this new classification scheme are in Wasson and Kallemeyn (2002).

NWA 468 and the closely related Antarctic iron GRV 98003 are plotted as large, lightly shaded triangles near the centers of the eight diagrams (Fig. 1). The two irons plot near each other on all diagrams except Ge-Au (Fig. 1c) and Ga-Au (Fig. 1d); GRV 98003 has Ga and Ge contents 5-10× lower than those in NWA 468. Wasson and Kallemeyn (2002) called these two irons the NWA 468 duo.

Two other ungrouped irons that plot relatively close are Ventura and Yamato 8451 (hereafter Y8451). The latter also contains silicates and was called a pyroxene pallasite by Boesenberg et al. (2000).

The subgroup that is nearest NWA 468 on most diagrams is sHL (shown as large gray squares in Fig. 1). The most significant difference between sHL and NWA 468 is that the Co values of NWA 468 are much higher. Although the Sb concentrations are somewhat higher in the NWA 468 duo than in sHL, the scatter in sHL is large, and the Sb-Au trend is ill defined. Two sHL members, Sombrerete and Lonaconing, plot near NWA 468 on most diagrams; Sombrerete is also very similar in O-isotopic composition (see below).

Figure 2 shows CI-chondrite- and Ni-normalized abundance ratios for the metal portion of NWA 468; the data are plotted in order of volatility increasing to the right. There is an overall tendency for the more volatile elements to be increasingly depleted, but superimposed on this trend are high abundance ratios of the common siderophiles Ni and Co, and the volatile siderophiles Au and As. Iron (a common siderophile) is 2-3× lower than Ni, Co, Au and As; Cu (a moderately volatile siderophile) is 5-6× lower than these elements.

Also shown in Fig. 2 is the metal composition of GRV 98003, the other member of the NWA 468 duo. Abundances of Pt, Ni, Co, Fe, Au, As and Cu in GRV 98003 are similar to those in NWA 468, but GRV 98003 has much lower abundances of two refractory siderophiles (Re and Ir), two volatile siderophiles (Ga and Ge), and Cr.

3.2 Bulk Composition of the Silicates

Figure 3 shows CI-chondrite- and Mg-normalized abundance ratios for the silicates. The elements in the silicate portion of NWA 468 are divided into two groups -- the lithophiles at the left and the siderophiles and chalcophiles at the right. Data are listed in Table 2. The abundance ratios in NWA 468 silicate are moderately high (1.8-2.0×CI) for the refractory lithophiles Sc and Ca, low for Al (0.19×CI), low (0.10-0.12×CI) for two of the light REE (Sm and Eu), but somewhat higher (0.26×CI) for La, and higher still (0.32-0.42×CI) for the heavy REE (Yb, Lu). The lowest REE value is that of Eu, interpretable as a small negative Eu anomaly.

The moderately volatile lithophiles show a progressive and substantial depletion with increasing volatility. However, Mn (0.86×CI) is nearly unfractionated, and the low abundances of Na (0.078×CI) and K (0.014×CI) are probably associated with loss of plagioclase (which also led to the depletion in Al) with minor volatility effects superposed.

Particularly enhanced are the non-volatile lithophiles V (3.8×CI) and Cr (5.4×CI), probably reflecting a chromite content in the analyzed sample appreciably greater than the 3.0 wt.% chromite in silicate clast A, which is itself equivalent to a Cr abundance ratio of ~2.6×CI and a V abundance ratio of

~1.3×CI (making the assumption that the V_2O_3 content of NWA 468 chromite is the same as that in ordinary chondrites, i.e., ~0.7 wt.%; Bunch et al., 1967).

Most siderophiles in the silicates form a relatively flat pattern at low abundances (0.06-0.08×CI), but Ir is significantly depleted (0.015×CI) as it is in the metal portion of NWA 468. The abundances of Fe, Se and Cu are enhanced (0.35-0.38×CI) relative to most siderophile elements, presumably reflecting relatively high modal abundances of troilite (FeS).

Because the O-isotopic composition of NWA 468 resembles that of CR, CH and some CV carbonaceous chondrites, as well as lodranites and acapulcoites (see next section), we compared the bulk compositions of these rocks to that of NWA 468.

The lithophile and siderophile abundance patterns of the silicates in NWA 468 do not resemble the relatively flat patterns of refractory lithophiles and refractory and common siderophiles in CH and CR chondrites (e.g., Wasson and Kallemeyn, 1990; Kallemeyn et al., 1994).

Acapulcoites also differ from NWA 468 in having relatively flat refractory lithophile patterns with only slight (factor of 1.4-2) depletions in moderately volatile Na and K (Kallemeyn and Wasson, 1985). Abundance ratios of volatile siderophiles and chalcophiles (As, Ga, Sb and Se) decrease with increasing volatility, a pattern very different from that of NWA 468 silicate.

Most lodranites have complex lithophile-element patterns (Fig. 4) consisting of low Al, higher abundances of Sc and Ca, lower and fractionated REE (replete with negative Eu anomalies) and low alkalies.

Because the concentrations of many elements are available for one reasonably typical lodranite, MAC 88177 (Table 2), we compare its elemental abundance pattern to that of NWA 468 silicate (Fig. 3). The lithophile patterns of both rocks have low Al, relatively high Sc and Ca, low and fractionated REE (with a negative Eu anomaly and heavy REE enrichment) and significant depletions in Na and K. Differences in the patterns include a high La/Sm ratio in NWA 468 but not in MAC 88177, and very high V and Cr in NWA 468. The rocks also have somewhat similar siderophile patterns: both have low Ir and relatively unfractionated abundances of Ru and common and volatile siderophiles except for high Fe and Cu. In contrast to NWA 468, the Se abundance in MAC 88177 is only slightly enhanced.

3.3 Oxygen-isotopic Composition of the Silicate

The O-isotopic composition of NWA 468 silicates ($\Delta^{17}O$ = -1.39‰ relative to SMOW; R.N. Clayton and T.K. Mayeda, pers. commun., 2001) lies outside the IAB range ($\Delta^{17}O$ = -0.30 to -0.62 ‰) given by Clayton and Mayeda (1996). Figure 5 shows that the composition of NWA 468 is fairly close to that of Sombrerete ($\Delta^{17}O$ = -1.39 ‰) as well as acapulcoites, e.g., ALH81187 ($\Delta^{17}O$ = -1.03 ‰), lodranites, e.g., Y-74357 ($\Delta^{17}O$ = -1.31 ‰), CR chondrites, e.g., EET87770 ($\Delta^{17}O$ = -1.22 ‰), CH chondrites, e.g., ALH85085 ($\Delta^{17}O$ = -1.62 ‰) and a few CV chondrites, e.g., Mokoia ($\Delta^{17}O$ = -2.74 ‰) (Clayton and Mayeda, 1996, 1999). Lodranite MAC 88177 has an O-isotopic composition ($\delta^{18}O$ = +3.52 ‰; $\delta^{17}O$ = +0.60 ‰; $\Delta^{17}O$ = -1.23 ‰) near that of NWA 468 and Sombrerete (Clayton and Mayeda, 1996). Slightly less similar in O-isotopic composition is the silicate-bearing iron Y8451 ($\Delta^{17}O$ = -0.77 ‰), which is similar to NWA 468 in metal composition. Vermillion ($\Delta^{17}O$ = -0.76 ‰) is related to Y8451, but less similar in metal composition to NWA 468.

3.4 Silicate Textures and Mineralogy

The largest sample of NWA 468 that we have seen (~22 cm^2; LC 1706) contains ~55 vol.% (~34 wt.%) silicate and ~45 vol.% (~66 wt.%) metallic Fe-Ni (Fig. 6). The silicate masses range from ~20 μm to ~4.5 cm in maximum dimension. The silicates are surrounded by metal; the metal-silicate interface is very irregular with diffuse peninsulas of silicates protruding into the metal from large adjacent silicate masses. The whole-rock texture shows multi-centimeter-size irregular silicate clasts surrounded by metal; also included in the metal are variable amounts of small silicate grains and clasts. Many metal regions between the large silicate clasts contain 25-50 vol.% silicate grains with mean dimensions of ~1 mm; a few centimeter-size patches are free of silicates.

Troilite is enriched near (but generally not at) the margins of many of the large silicate clasts. In a typical occurrence (silicate clast B), troilite occurs as an elongated spidery network of veins (typically 20-400-μm thick) and veinlets (typically 0.5-3-μm thick) located within the clast ~400 μm from the clast/metal boundary (Fig. 7a). Some of the veinlets are connected to curvilinear trails of small (1-4-μm-size) troilite blebs. The troilite network runs subparallel to the clast boundary and, in a few cases, a patch of troilite occurs at the boundary. The region within the clast containing the troilite network is 0.5-15-mm thick and

consists of 25-40 vol.% troilite, 60-75 vol.% silicate, and no metallic Fe-Ni. A few spidery troilite networks also penetrate the clast interior, forming quasi-linear features.

The modal abundances of two silicate clasts are listed in Table 3; however, only clast A was studied in thin section. Although clast A has chondritic minerals, its modal mineralogy differs significantly from the normative mineralogy of ordinary chondrites (e.g., Table 4 of Dodd, 1981). For example, relative to H chondrites, clast A is appreciably richer in low-Ca pyroxene (34.8 vs. 24.5 wt.%), diopside (10.8 vs. 4.0 wt.%) and chromite (3.0 vs. 0.6 wt.%) and poorer in feldspar (1.3 vs. 10.0 wt.%) and metallic Fe-Ni (6.5 vs. 18.6 wt.%). These modal mineralogical differences reflect the bulk compositional differences between clast A and chondrites (e.g., CI; Fig. 3).

The silicates in clast A have an allotriomorphic-granular texture consisting mainly of interlocking anhedral grains of mafic silicates. Individual olivine and low-Ca pyroxene grains range in size from ~0.3 to ~3.5 mm. Modal analysis shows that ~30% of the low-Ca pyroxene in clast A is monoclinic as indicated by its well-developed polysynthetic twinning and inclined extinction (Fig. 7b). Elongated curved low-Ca pyroxene bars (typically 30×600 μm) extend through some olivine grains that are adjacent to large low-Ca pyroxene grains. Most low-Ca pyroxene grains have poikilitic textures and contain small olivine chadacrysts ranging in size from 15 to 150 μm.

Olivine ranges in composition from $Fa_{4.0}$ to $Fa_{7.1}$ and averages $Fa_{5.3}$. It contains low concentrations of CaO (~0.05 wt.%) and moderate concentrations of Cr_2O_3 (0.10 wt.%) and MnO (0.39 wt.%) (Table 4). Low-Ca pyroxene is more homogeneous in composition than olivine, ranging from $Fs_{8.6}$ to $Fs_{9.4}$. The Wo component ranges from 1.8 to 2.1 mol%. Minor concentrations (in wt.%) of Cr_2O_3 (0.41 wt.%), Al_2O_3 (0.27 wt.%) and MnO (0.48 wt.%) are present (Table 4). Diopside averages $Fs_{3.7}Wo_{45.4}$ and contains appreciable Cr_2O_3 (1.0 wt.%) and lower concentrations of Al_2O_3 (0.64 wt.%) and MnO (0.31 wt.%).

Most plagioclase grains are 10-20 μm in size and located at the boundary between diopside and low-Ca pyroxene. In some cases, small (2-10 μm) rounded, euhedral or anhedral grains of chromite are associated with the plagioclase grains. A few plagioclase grains (including rare larger grains up to 40 μm in maximum dimension) are completely surrounded by low-Ca pyroxene. Plagioclase is moderately sodic in composition. It averages $Ab_{78.7}Or_{2.6}$ and contains minor concentrations of FeO (0.40 wt.%).

Most chromite grains are angular and anhedral and range in maximum dimension from 30-750 μm. There are two distinct populations of chromite: small (generally <20 μm) chromite grains (many of which are associated with troilite), contain higher concentrations of SiO_2, FeO and, possibly some Fe_2O_3, and lower concentrations of MgO than large (100-300 μm) chromite grains (which occur within silicate and at the margins of metallic Fe-Ni grains). Although there is some overlap, CaO tends to be higher and Cr_2O_3 lower in the small chromite grains. The two populations of chromite contain similar concentrations of Al_2O_3 and TiO_2 (Table 4).

Other opaque phases in the silicate inclusion include kamacite, taenite, plessite, troilite, schreibersite and limonite; the latter phase was produced by terrestrial weathering. Individual troilite grains are very irregular; many have multiple appendages extending 50-400 μm through the surrounding silicate (Fig. 7c). Metallic Fe-Ni occurs as relatively small, elongated grains (typically 200-300 μm in maximum dimension) and as large, disconnected, moderately elongated, vein-like masses. Small (10-50 μm) troilite patches occur along the margins of some large metal grains. Rare, small (typically 40-100-μm-size) patches of schreibersite occur at the interface of metal and silicate. Silicates form protruding peninsulas into some of the larger metal grains; a few 100-μm-size patches of silicate have broken off from the peninsulas and are now completely surrounded by metal. These silicates include isolated olivine grains, poikilitic pyroxene grains and granular olivine-pyroxene assemblages.

Portions of the margins of many troilite grains have been melted. There are ~50-μm-size clouds of wormy 2-8-μm troilite particles adjacent to many of the large troilite grains (Fig. 7d). The clouds also occur adjacent to some small chromite grains; some chromite grains are nearly completely surrounded by the troilite clouds. Some clouds consist of small wormy troilite and chromite grains. One such 100-μm-size cloud is adjacent to a 70-μm troilite-chromite assemblage and surrounds a 20-μm quasi-equant chromite grain with a highly irregular margin. It is apparent that the adjacent troilite is the source of the wormy troilite and that the chromite in the center of the cloud is the source of the wormy chromite grains. It seems very likely that these textures resulted from a late shock-mobilization event.

Thin (0.5-μm-thick) veins of troilite and chromite extend through many of the silicate grains. Some of the troilite veins are blebby and consist of 1-2-μm-size individual troilite grains. These curvilinear

trails of troilite grains cause moderate silicate darkening. Troilite veins also cut through some chromite grains.

The clouds of wormy troilite grains and the veins and curvilinear trails of troilite and chromite are responsible for darkening of the silicate clasts (Rubin, 1992) and probably resulted from a late-stage shock event.

3.5 Metallography

The mean Ni content of the metal is 119 mg/g. Several millimeters away from the silicate inclusions in NWA 468, the metal consists of ~5-mm-wide regions of duplex plessite composed of 50-300-μm-size spark- and spindle-shaped kamacite grains that have nucleated on schreibersite. These duplex plessite regions represent original γ crystals. Adjacent plessite regions contain kamacite spindles with different orientations.

The kamacite grains in the duplex plessite regions occur amidst fine-grained, irregularly shaped plessitic fields (Fig. 8a) that are themselves rimmed with 2-4-μm-thick rinds of taenite with ~35 wt.% Ni. The large duplex plessite regions are separated by 3-8-mm-long, 50-150-μm-wide curvilinear shafts of schreibersite flanked by 40-80-μm-thick bands of swathing kamacite (Fig. 8b).

Plessite fields adjacent to the silicate inclusions are much finer grained than the large plessite fields several millimeters away from the silicates, but are likewise surrounded by ~2-μm-thick rims of taenite with ~29-35 wt.% Ni and <0.04 - 0.06 wt.% Co. Kamacite grains within these finer-grained plessite regions are typically 5-25 μm in size. Plessite fields distributed among the silicate inclusions are 50-500 μm in maximum size. These fields are similarly fine grained, but their taenite rims are generally much thicker (2-150 μm) than those of plessite regions outside the silicate inclusions. Some of the taenite rims around those plessite regions located among the silicate inclusions extend from the plessite regions to the silicate inclusions; other taenite rims connect adjacent regions of plessite.

Kamacite grains (including swathing kamacite and sparks and spindles amidst the fine-grained plessitic regions) are fairly homogeneous in composition, averaging 7.2 wt.% Ni and 0.62 wt.% Co. Most troilite grains are Ni-free (<0.05 wt.%), although rare small (non-wormy) grains contain 0.1-0.2 wt.% Ni. The troilite Cr concentration is somewhat variable, ranging from 0.59-1.2 wt.% and averaging 0.75 wt.%. Schreibersite is Ni-rich, averaging 32.5 wt.% Ni; Co contents are <0.04 wt.%, but there are small concentrations of S (0.05-0.10 wt.%; mean 0.08 wt.%).

A few silicate inclusions have 10-300-μm-size schreibersite grains at their margins. Bands of swathing kamacite (50-250 μm thick) surround all of the silicate inclusions, every grain of schreibersite and each region of plessite nestled among the silicate inclusions. Although chromite and troilite occur within the silicate inclusions, very few grains of these phases occur at the silicate-metal interface.

3.6 Weathering

Clasts A and B contain 2.7 and 0.5 vol.% limonite, respectively (Table 3). Limonite is most abundant near the surface of the meteorite. It also occurs as overgrowths on many of the schreibersite shafts (and surrounding swathing kamacite) that separate duplex plessite regions. Limonite is rare in the meteorite interior. Although the weathering scale of Wlotzka (1993) was designed for ordinary chondrites, it can be applied to silicate-rich metal-bearing meteorites. On this basis, NWA 468 would be weathering stage W1.

4. DISCUSSION

4.1 Comparison of NWA 468 Silicates to Inclusions in Iron and Stony-iron Meteorites

Iron meteorite groups that contain significant amounts of silicates include the IAB complex (Wasson and Kallemeyn, 2002) and the IIE irons. IIE silicates differ significantly from those in NWA 468 in mineralogy, bulk chemistry and O-isotopic composition. More closely related meteorites are discussed below.

4.1.1 IAB iron complex

Many of the ~160 IAB-complex irons plotted in Fig. 1 contain silicate inclusions. Among the members of the main group and the three low-Au subgroups, fine silicates are nearly ubiquitous; about 15% of these irons contain coarse (>2 mm) silicate aggregates. As summarized by Benedix et al. (2000), most of these aggregates are chondritic in mineralogical and chemical composition. IAB olivine spans a range ($Fa_{0.8\text{-}8.0}$) (Benedix et al., 2000) that includes the mean composition of NWA 468 olivine ($Fa_{5.3}$).

In every investigated silicate in the IAB main group and the low-Au subgroups and grouplets, the $\Delta^{17}O$ value is within the carbonaceous-chondrite range, i.e., $-0.3‰ < \Delta^{17}O < -0.7‰$.

The fractionation trends within the five subgroups of the IAB complex (Fig. 1) are generally subparallel to those in the main group (MG). Wasson and Kallemeyn (2002) interpreted the MG trends in terms of a single-step, solid-melt segregation model, with the high-Ni irons having high melt contents and with the low-Ni irons having high solid contents. In order to explain why the fine silicates were not able to separate buoyantly, Wasson and Kallemeyn (2002) suggested that the melt was initially rich in crystallization nuclei, and that it cooled (and crystallized) quickly as a result of conduction of heat into adjacent cooler silicates. They argued that such rapid heating and cooling is not possible in an internally heated asteroid, but that impact heating must have been involved in the production of the members of the IAB complex.

4.1.2 Sombrerete, Y8451, GRV 98003, Ventura and Lonaconing

Sombrerete (a member of subgroup sHL) is closest to NWA 468 in O-isotopic composition ($\Delta^{17}O$ = -1.39‰; Clayton and Mayeda, 1996) (Fig. 5). The silicate inclusions in Sombrerete are rounded and consist of major quench-textured albitic glass, chlorapatite and orthopyroxene, minor chromite, ilmenite, tridymite and Ti-rich kaersutite [an amphibole of formula $NaCa_2(Mg,Fe)_4Ti(Si_6Al_2)O_{22}(OH)_2$], trace amounts of rutile, and no olivine (Prinz et al., 1982). In contrast, NWA 468 contains crystalline plagioclase and abundant olivine, but no phosphate, tridymite, rutile or kaersutite. Sombrerete is a partially differentiated rock that may have formed in a manner analogous to that of IIE irons (which were modeled by Rubin et al.,1986 and Wasson and Wang,1986 as having been produced by impact-induced preferential melting of plagioclase). If so, it is possible that the parent material of Sombrerete had a chondritic composition closely related to that of the precursors of NWA 468.

The O-isotopic composition of Y8451 ($\Delta^{17}O$ = -0.77‰; Clayton and Mayeda, 1996) is relatively similar to that of NWA 468. Y8451, which has been called a pyroxene pallasite, consists of 57 vol.% rounded to subangular silicate masses and 43 vol.% metallic Fe-Ni (Yanai and Kojima, 1995; Boesenberg et al., 2000). Silicates include (in vol.%): 97% olivine, 2.0% low-Ca orthopyroxene, 0.4% low-Ca clinopyroxene, 0.4% augite, 0.1% merrillite and trace amounts of chromite (Boesenberg et al., 2000). Although the proportions of phases differ significantly, the silicate mineralogy of Y8451 is similar to that of NWA 468.

The nearest compositional relative of the metal of NWA 468 is the iron meteorite GRV 98003; the chief differences are the 5-10× lower Ga and Ge and 50× lower Ir concentrations in GRV 98003. Our observations of this iron show it to have a sharply defined plessitic octahedrite structure. Like NWA 468, GRV 98003 plessite contains kamacite sparks and spindles, many of which contain a nugget of schreibersite in the center; it is clear that in both meteorites, the kamacite nucleated on schreibersite grains. The similarities in metal texture and composition suggest that NWA 468 and GRV 98003 formed by similar processes from similar precursor materials.

Lonaconing (a member of the sHL subgroup) and Ventura are also quite close to NWA 468 in metal composition (Fig. 1). The major difference between NWA 468 and Ventura, GRV 98003 and Lonaconing is that silicates have only been reported in NWA 468.

4.2 Comparison of NWA 468 Silicates to Possible Chondritic and Subchondritic Parental Materials

The CR carbonaceous chondrites ($\Delta^{17}O$ = -0.96 to -2.42 ‰), the CH chondrites (-1.25 to -1.62 ‰) and the subchondritic Iodranites and acapulcoites ($\Delta^{17}O$ = -0.85 to -1.49 ‰ and -0.85 to -1.22 ‰, respectively) have O-isotopic compositions similar to that of NWA 468 silicates ($\Delta^{17}O$ = -1.39‰) (Fig. 5). Like NWA 468, these groups have chondritic silicate mineralogy (olivine, low-Ca pyroxene, high-Ca pyroxene, plagioclase) and are rich in metallic Fe-Ni: CR, ~9-17 wt.% metal (Weisberg et al., 1993); CH, ~40 wt.% (in ALH85085; Grossman et al., 1988; Scott, 1988; Weisberg et al., 1988); Iodranites, ~20-38 wt.% (in most unweathered samples; McCoy et al., 1997a); acapulcoites, ~23 wt.% (in the Acapulco fall; Palme et al., 1981). The CR chondrites are a more plausible source than CH chondrites for the precursor materials of NWA 468 because of the low bulk S contents of CH chondrites (e.g., 0.6 wt.% in ALH85085 host material; Grossman et al., 1988).

4.3 Cooling History Inferred from Low-Ca Clinopyroxene

Low-Ca pyroxene that exhibits polysynthetic twinning and inclined extinction occurs in the silicate inclusions in NWA 468 (and in the Iodranite MAC 88177; our observations). These petrographic properties indicate that this phase is low-temperature clinopyroxene. Low-Ca clinopyroxene occurs as phenocrysts in pyroxene-bearing chondrules in highly unequilibrated type-3 chondrites (e.g., Fig. 4.5 of Dodd, 1981), but it does not occur in unshocked, unbrecciated type-5 and -6 ordinary chondrites (e.g.,

Van Schmus and Wood, 1967); orthopyroxene is the sole low-Ca pyroxene phase in these rocks. This is because thermal metamorphism and slow cooling transform low-Ca clinopyroxene into orthopyroxene.

The presence of low-Ca clinopyroxene in the silicate inclusions in NWA 468 (and in the "pyroxene pallasite" Y8451; Boesenberg et al., 2000) indicates that the silicate inclusions of these meteorites experienced rapid cooling. Smyth (1974) showed that twinned low-temperature (primitive) clinoenstatite forms from protoenstatite in a quench accomplished within a few seconds or less. The stability field of protoenstatite is restricted to the enstatite corner of the pyroxene quadrilateral: the field ranges in mol% Fs from 0 to 13 and in mol% Wo from 0 to 2 (Smyth, 1974). The composition of the low-Ca pyroxene in NWA 468 is marginally within these ranges ($Fs_{8.6\text{-}9.4}$ $Wo_{1.8\ to\ 2.1}$) and it is conceivable that the low-Ca clinopyroxene formed from protoenstatite by such a rapid quench. However, even the small amount of Ca in the low-Ca pyroxene in NWA 468 may be sufficient to have prevented the phase from entering the protoenstatite field (J.R. Smyth, pers. commun., 2001). In that case, it probably formed from high-temperature clinopyroxene by cooling from high temperatures (≥~1000°C; Perrotta and Stephenson, 1965) in less than a few hours (J.R. Smyth, pers. commun., 2001); at slower cooling rates the phase would have reverted to orthopyroxene (Smyth, 1974). Low-temperature, low-Ca clinopyroxene is stabilized relative to orthopyroxene by shear stress lasting as briefly as 1 s (Coe, 1970); it is plausible that shear stresses involved in the impact that formed NWA 468 helped to stabilize the low-Ca clinopyroxene.

The low-Ca clinopyroxene grains may have formed from relict orthopyroxene by shock heating and quenching. Hornemann and Müller (1971) and Stöffler et al. (1991) found that clinopyroxene lamellae form within orthopyroxene at shock pressures of ~5 GPa. Rubin et al. (1997) found that low-Ca clinopyroxene grains are common in ordinary chondrites of shock stage ≥S3. Alternatively, the low-Ca clinopyroxene may have formed from a melt during quenching (as it did in many pyroxene-bearing chondrules; e.g., Alexander, 1994). It may be necessary to perform transmission electron microscope (TEM) studies of the low-Ca clinopyroxene in NWA 468 to determine the cooling history of this meteorite.

At temperatures below ~600°C, low-temperature, low-Ca clinopyroxene may be stable over geologic time periods (Smyth, 1974). Thus, it may survive despite slow cooling below this temperature (consistent with the interpretation of the metallography; see below) or even low-temperature metamorphism causing measurable effects in other phases such as olivine.

The mean low-Ca pyroxene Fs value (~9 mol%) in NWA 468 is out of equilibrium with the olivine Fa value (5.3 mol%); in equilibrated assemblages such as metamorphosed ordinary chondrites, the Fa value is greater than the Fs value (e.g., Keil and Fredriksson, 1964). We interpret this to indicate that olivine continued to react with a reducing agent in the NWA 468 assemblage down to temperatures below the low-Ca pyroxene diffusional blocking temperature.

4.4 Cooling History Inferred from Metallography

As indicated above, the metal portion of NWA 469 contains 119 mg/g Ni. Several millimeters away from the silicate inclusions, the metal in NWA 468 consists of ~5-mm-wide regions of duplex plessite representing 5-mm-wide original γ crystals. Iron meteorites with 119 mg/g Ni and ~5-mm-wide γ crystals such as NWA 468 must have cooled relatively rapidly at temperatures above ~660°C. Appreciably slower cooling would have resulted in coarser original γ crystals. On the other hand, an iron meteorite with a Ni concentration near that of NWA 468 that contains sparks and spindles of kamacite enclosed in a matrix of fine plessite must have cooled moderately slowly at temperatures <~660°C. This is the case for the Wiley IIC iron, which resembles NWA 468 in Ni content and structure; as in NWA 468, Wiley's kamacite sparks and spindles appear to have nucleated on schreibersite (Buchwald, 1975). (Rapid cooling at temperatures <~660°C would have resulted in finer-grained plessitic regions.) We can thus infer a two-stage cooling history for NWA 468: relatively rapid cooling at temperatures >660°C and moderately slow cooling at lower temperatures.

4.5 Metal/sulfide Fractionation

Plausible precursor materials for NWA 468 (e.g., CR chondrites) probably contained substantial amounts of metallic Fe-Ni (~10-20 wt.%) and troilite (~2-5 wt.%). The metal in NWA 468 has a high Ni content of ~119 mg/g, a value that would be found in relatively oxidized chondrites (e.g., in chondrites containing 6-10 wt.% metallic Fe-Ni). Because the silicate inclusions in NWA 468 contain relatively little metal (i.e., 2.9 vol.% in clast A; <0.1 vol.% in clast B), we infer that the silicate inclusions lost their metal (and most of their FeS) during an episode of impact melting. Silicate and metal-sulfide would have formed immiscible liquids; if viscosities were low enough and channels were available, the much denser metal-sulfide melt would have tended to separate from the silicate. Such gravitational separation (or an

episode of impact-driven separation) is consistent with the low siderophile abundances in the silicate (Fig. 3). Some of the small silicate clasts seem to have been crushed and invaded subsequently (perhaps during a second impact event) by molten metal.

Molten sulfide is completely miscible in a metal melt at high temperatures. Thus, if gravitational separation of the metal occurred, the sulfide should also have been lost. We observed relatively high sulfide abundances in clasts A and B (7.9 and 8.0 wt.%, respectively) and enrichment in sulfide near the margins of clast B (Fig. 6). The S thus seems to have been reintroduced to the NWA 468 silicates. We considered three models: invasion by a residual S-rich eutectic melt, by impact-mobilized FeS containing minimal amounts of metal, or by an S_2-rich vapor. These mechanisms could have formed the spidery network of troilite veins near the margins of clast B, although the petrographic evidence favors a melt.

The FeS/metal ratio in clast B (>80 g/g) is much higher than the eutectic ratio (7.5 g/g; Brandes and Brook, 1992). It thus appears that FeS cannot have been reintroduced into the silicate in the form of a eutectic melt. Deposition of an S_2-rich vapor by condensation on and reaction with residual metal could account for the high FeS/metal ratio; however, this model requires a spidery network of metal to have already been in place. We therefore consider the most plausible model to involve shock mobilization of FeS that was relatively free of metal.

These models account for the high abundances of Fe and Se relative to the more-siderophile elements in the silicate (Fig. 3). The high abundance of Cu in the silicate-rich sample probably reflects a high concentration of Cu in troilite (or in the vapor). Silicate melting, separation of a metal-sulfide melt, and reintroduction of sulfide into the silicate via a vapor phase are processes postulated previously for the Portales Valley and Smyer H-chondrite impact-melt breccias (Rubin et al., 2001; Rubin, 2002).

The Ni-normalized siderophile abundance pattern of the silicates (Fig. 3) differs from that of the metal portion of NWA 468 (Fig. 2). The metal associated with the silicates has much lower Ir and much higher Fe, Cu, Ga and Sb. The chalcophile element Se is also much higher in the silicates than in the metal; a rough estimate of the Se concentration in the metal is ~0.1 μg/g (based on the observed low modal abundance of troilite in the metal and the cosmic S/Se ratio). The respective silicate and metal element/Ni CI-chondrite-normalized abundance ratios are: Ir/Ni (0.16, 0.55), Fe/Ni (4, 0.4), Cu/Ni (4, 0.2), Ga/Ni (0.8, 0.3), Sb/Ni (0.9, 0.25) and Se/Ni (4.3, $\sim 5\times10^{-4}$).

Chondrites tend to show progressive depletions of siderophile elements with increasing volatility (e.g., Fig. 3 of Wasson and Kallemeyn, 1988). The siderophile abundance pattern of the metal portion of NWA 468 can be interpreted as indicating that a component rich in Fe and Cu (and presumably S and Se; not determined) was removed from metal that previously had an approximately chondritic composition. We suggest that this is best accomplished by volatilization of FeS and CuS.

The silicate siderophile pattern shows a complementary enrichment in Fe, Cu and Se, most likely resulting from the acquisition of volatiles lost during the formation of the metal portion. The large depletion of Ir relative to Ni and more volatile siderophiles could be due either to partial vaporization and removal of common and volatile siderophiles as a gas, or complete vaporization followed by fractional condensation, a process akin to that described by Widom et al. (1986).

4.6 Lithophile Fractionations: Constraints on the Formation of NWA 468, Acapulcoites and Lodranites

CH and CR carbonaceous chondrites, NWA 468 silicates, and the lodranite and acapulcoite groups contain abundant metallic Fe-Ni and have related O-isotopic compositions. Impact melting of a metal-rich carbonaceous chondrite (such as a member of the CR group) could give rise to a rock with the basic texture and chemical composition of NWA 468. The low abundances of Al, Na and K in NWA 468 silicates (Fig. 3) indicate that plagioclase was lost from the melt. This could have occurred during preferential shock melting and mobilization of plagioclase (which has a low impedance to shock compression; Schaal et al., 1979) from NWA 468 precursors.

The V-shaped REE pattern of NWA 468 silicates resembles that of the mean of two MAC 88177 specimens analyzed at UCLA and plotted in Fig. 3; it also resembles the best estimate of the REE pattern of the non-polymict ureilite Novo Urei (Fig. 4 of Warren and Kallemeyn, 1989). However, Zipfel and Palme (1993) analyzed a different specimen of MAC 88177 and did not find a V-shaped REE pattern; their data show LREE depletions and a negative Eu anomaly. It is unclear how these REE patterns formed.

The low siderophile abundances of the silicate portion of NWA 468 result from separation of metal from silicate; the high Ni-normalized Fe, Cu and Se abundances in the silicate indicate reintroduction of sulfide.

NWA 468 is an ungrouped member of the IAB complex, the members of which are inferred to have formed by impact melting on carbonaceous-chondrite asteroids (Wasson and Kallemeyn, 2002). Our proposed impact-melt origin for NWA 468 is consistent with this view, but NWA 468 silicates are more fractionated than most coarse IAB silicates. The impact-melting model for IAB-complex irons differs from that of Benedix et al. (2000) who postulated that an internal heat source, probably ^{26}Al, was responsible for the melting.

The similar abundance patterns of the lodranites (particularly MAC 88177) to NWA 468 silicates (Figs. 3, 4) suggest that lodranites may have formed by a process analogous to that which formed NWA 468. Consistent with this suggestion is the occurrence of moderately coarse grains of low-Ca clinopyroxene in both NWA 468 and MAC 88177 (this study). Lodranites consist of homogeneously distributed silicate grains and submillimeter-size sulfide and metal grains and aggregates (e.g., Fig. 1a of McCoy et al., 1997a) and may have formed by an impact melting and quenching process that involved less separation of metal from silicates than experienced by NWA 468. The high Fe and Cu and enhanced Se in MAC 88177 suggest that lodranites lost some metal and sulfide and then, like NWA 468, experienced some re-introduction of sulfide, perhaps as an FeS melt or an S_2-rich vapor.

This model of lodranite formation differs from that of McCoy et al. (1997a,b) who proposed that lodranites (and acapulcoites) formed by low-degree partial melting by an internal heat source. Subsequent annealing of lodranites and acapulcoites may have devitrified any glass that had formed and caused the rocks to acquire their recrystallized textures. The major bulk compositional differences between NWA 468 silicates and the MAC 88177 lodranite are the higher V and Cr abundances in NWA 468. These probably reflect a higher modal abundance of chromite in NWA 468 silicates (1.4-3.0 wt.%) than in MAC 88177 (1.1 wt.%; Table 3).

Acknowledgements--We are greatly indebted to David Gregory for donating samples of NWA 468 to the UCLA collection. We thank R.N. Clayton and T.K. Mayeda for permission to cite their unpublished O-isotopic composition data. We are grateful to J.R. Smyth for information on the properties of low-Ca clinopyroxene. Reviews by J. Zipfel, T.J. McCoy and an anonymous referee were very helpful in revising the manuscript. This research was mainly supported by NASA grant NAG5-4331 (J.T. Wasson).

REFERENCES

Alexander C. M. O. (1994) Trace element distributions within ordinary chondrite chondrules: Implications for chondrule formation conditions and precursors. *Geochim. Cosmochim. Acta* **58**, 3451-3467.

Baedecker P. A. and Grossman J. N. (1989) The computer analysis of high resolution gamma-ray spectra from instrumental neutron activation analysis experiments: U.S. Geol. Surv. Open File Report 89-454, 88 pp.

Benedix G. K., McCoy T. J., Keil K., and Love S. G. (2000) A petrologic study of the IAB iron meteorites: Constraints on the formation of the IAB-winonaite parent body. *Meteorit. Planet. Sci.* **35**, 1127-1141.

Bild R. W. (1977) Silicate inclusions in group IAB irons and a relation to the anomalous stones Winona and Mt. Morris (Wis.). *Geochim. Cosmochim. Acta* **41**, 1439-1456.

Boesenberg J. S., Davis A. M., Prinz M., Weisberg M. K., Clayton R. N. and Mayeda T. K. (2000) The pyroxene pallasites, Vermillion and Yamato 8451: Not quite a couple. *Meteorit. Planet. Sci.* **35**, 757-769.

Brandes E. A. and Brook G. B., editors (1992) Equilibrium diagrams, pp. 11-1--11-496. In *Smithells Metals Reference Book*, 7th edition, Butterworth-Heinemann, Oxford.

Buchwald V. F. (1975) *Handbook of Iron Meteorites*, Univ. Calif. Press, Berkeley, 1418 pp.

Bunch T. E., Keil K. and Snetsinger K. G. (1967) Chromite composition in relation to chemistry and texture of ordinary chondrites. *Geochim. Cosmochim. Acta* **31**, 1569-1582.

Choi B., Ouyang X., and Wasson J. T. (1995) Classification and origin of IAB and IIICD iron meteorites. *Geochim. Cosmochim. Acta* **59**, 593-612.

Clayton R. N. and Mayeda T. K. (1963) The use of bromine pentafluoride in the extraction of oxygen from oxides and silicates for isotopic analysis. *Geochim. Cosmochim. Acta* **27**, 43-52.

Clayton R. N. and Mayeda T. K. (1996) Oxygen isotope studies of achondrites. *Geochim. Cosmochim. Acta* **60**, 1999-2017.

Clayton R. N. and Mayeda T. K. (1999) Oxygen isotope studies of carbonaceous chondrites. *Geochim. Cosmochim. Acta* **63**, 2089-2104.

Clayton R. N., Onuma N., and Mayeda T. K. (1976) A classification of meteorites based on oxygen isotopes. *Earth Planet. Sci. Lett.* **30**, 10-18.

Coe R. S. (1970) The thermodynamic effects of shear stress on the ortho-clino inversion in enstatite and other coherent phase transitions characterized by a finite simple shear. *Contrib. Mineral. Petrol.* **26**, 247-264.

Dodd R. T. (1981) *Meteorites-- A Petrologic-Chemical Synthesis*. Cambridge, 368 pp.

Dreibus G., Palme H., Spettel B., Zipfel J. and Wänke H. (1995) Sulfur and selenium in chondritic meteorites. *Meteorit. Planet. Sci.* **30**, 439-445.

Grossman J. N. and Zipfel J. (2001) The Meteoritical Bulletin, No. 85, 2001 September. *Meteorit. Planet. Sci.* **36**, A293-A322.

Grossman J. N., Rubin A. E., and MacPherson G. J. (1988) ALH85085: A unique volatile-poor carbonaceous chondrite with possible implications for nebular fractionation processes. *Earth Planet. Sci. Lett.* **91**, 33-54.

Haramura H., Kushiro I. and Yanai K. (1983) Chemical compositions of Antarctic meteorites I. *Mem. Nat. Inst. Polar Res.* **30**, 109-121.

Hornemann U. and Müller W. F. (1971) Shock-induced deformation twins in clinopyroxene. *Neues Jahrb. Mineral.* **6**, 247-256.

Kallemeyn G. W. and Wasson J. T. (1985) The compositional classification of chondrites: IV. Ungrouped chondritic meteorites and clasts. *Geochim. Cosmochim. Acta* **49**, 261-270.

Kallemeyn G. W., Rubin A. E., Wang D., and Wasson J. T. (1989) Ordinary chondrites: Bulk compositions, classification, lithophile-element fractionations, and composition-petrographic type relationships. *Geochim. Cosmochim. Acta* **53**, 2747-2767.

Kallemeyn G. W., Rubin A. E. and Wasson J. T. (1994) The compositional classification of chondrites: VI. The CR carbonaceous chondrite group. *Geochim. Cosmochim. Acta* **58**, 2873-2888.

Keil K. and Fredriksson K. (1964) The iron, magnesium, and calcium distribution in coexisting olivines and rhombic pyroxenes of chondrites. *J. Geophys. Res.* **69**, 3487-3515.

Kracher A. (1974) Untersuchungen am Landes Meteorit. In *Analyse Extraterrestrischen Materials* (eds. W. Kiesl and H. Malissa, Jr.), pp. 315-326. Springer, New York.

McCoy T. J., Keil K., Clayton R. N., Mayeda T. K., Bogard D. D., Garrison D. H. and Wieler R. (1997a) A petrologic and isotopic study of lodranites: Evidence of early formation as partial melt residues from heterogeneous precursors. *Geochim. Cosmochim. Acta* **61**, 623-637.

McCoy T. J. Keil K., Muenow D. W., Wilson L. (1997b) Partial melting and melt migration in the acapulcoite-lodranite parent body. *Geochim. Cosmochim. Acta* **61**, 639-650.

Nagahara H. and Ozawa K. (1986) Petrology of Yamato-791493, "lodranite": melting, crystallization, cooling history, and relationship to other meteorites. *Mem. Nat. Inst. Polar Res.* **41**, 181-205.

Palme H., Schultz L., Spettel B., Weber H. W., Wänke H., Michel-Levy M. C., and Lorin J. C. (1981) The Acapulco meteorite: chemistry, mineralogy and irradiation effects. *Geochim. Cosmochim. Acta* **45**, 727-752.

Perrotta A. J. and Stephenson D. A. (1965) Clinoenstatite, high-low inversion. *Science* **148**, 1090-1091.

Prinz M., Nehru C. E., and Delaney J. S. (1982) Sombrerete: An iron with highly fractionated amphibole-bearing Na-P-rich silicate inclusions (abstract). *Lunar Planet. Sci.* **13**, 634-635.

Rubin A. E. (1992) A shock-metamorphic model for silicate darkening and compositionally variable plagioclase in CK and ordinary chondrites. *Geochim. Cosmochim. Acta* **56**, 1705-1714.

Rubin A. E. (2002) Smyer H-chondrite impact-melt breccia and evidence for sulfur vaporization. *Geochim. Cosmochim. Acta* **66**, 699-711.

Rubin A. E., Jerde E. A., Zong P., Wasson J. T., Westcott J. W., Mayeda T. K., and Clayton R. N. (1986) Properties of the Guin ungrouped iron meteorite: The origin of Guin and of group-IIE irons. *Earth Planet. Sci. Lett.* **76**, 209-226.

Rubin A. E., Scott E. R. D. and Keil K. (1997) Shock metamorphism of enstatite chondrites. *Geochim. Cosmochim. Acta* **61**, 847-858.

Rubin A. E., Ulff-Møller F., Wasson J. T., and Carlson W. D. (2001) The Portales Valley meteorite breccia: Evidence for impact-induced melting and metamorphism of an ordinary chondrite. *Geochim. Cosmochim. Acta* **65**, 323-342.

Schaal R. B., Hörz F., Thompson T. D. and Bauer J. F. (1979) Shock metamorphism of granulated lunar basalt. *Proc. Lunar Planet. Sci. Conf.* **10th**, 2547-2571.

Scott E. R. D. (1982) Origin of rapidly solidified metal-troilite grains in chondrites and iron meteorites. *Geochim. Cosmochim. Acta* **46**, 813-823.

Scott E. R. D. (1988) A new kind of primitive chondrite, Allan Hills 85085. *Earth Planet. Sci. Lett.* **91**, 1-18.

Smyth J. R. (1974) Experimental study of the polymorphism of enstatite. *Amer. Mineral.* **59**, 345-352.

Stöffler D., Keil K., and Scott E. R. D. (1991) Shock metamorphism of ordinary chondrites. *Geochim. Cosmochim. Acta* **55**, 3845-3867.

Torigoye N., Yamamoto K., Misawa K. and Nakamura M. (1993) Composition of REE, K, Rb, Sr, Ba, Mg, Ca, Fe, and Sr isotopes in antarctic "unique" meteorites. *Proc. NIPR Symp. Ant. Met.* **6**, 100-119.

Ulff-Møller F., Choi B.-G., Rubin A. E., Tran J., and Wasson J. T. (1998) Paucity of sulfide in a large slab of Esquel: New perspectives on pallasite formation. *Meteorit. Planet. Sci.* **33**, 331-227.

Van Schmus W. R. and Wood J. A. (1967) A chemical-petrologic classification for the chondritic meteorites. *Geochim. Cosmochim. Acta* **31**, 747-765.

Warren P. H. and Kallemeyn G. W. (1989) Geochemistry of polymict ureilite EET83309, and a partially-disruptive impact model for ureilite origin. *Meteoritics* **24**, 233-246.

Wasson J. T. (1985) *Meteorites: Their Record of Early Solar-System History*. Freeman, New York, 267 pp.

Wasson J. T. and Kallemeyn G. W. (1988) Compositions of chondrites. *Philos. Trans. R. Soc. London* **A325**, 535-544.

Wasson J. T. and Kallemeyn G. W. (1990) Allan Hills 85085: A subchondritic meteorite of mixed nebular and regolithic heritage. *Earth Planet. Sci. Lett.* **101**, 148-161.

Wasson J. T. and Kallemeyn G. W. (2002) The IAB iron-meteorite complex: A group, five subgroups, numerous grouplets, closely related, mainly formed by crystal segregation in rapidly cooling melts. *Geochim. Cosmochim. Acta* **66**, in press.

Wasson J. T. and Schaudy R. (1971) The chemical classification of iron meteorites -- V Groups IIIC and IIID and other irons with germanium concentrations between 1 and 25 ppm. *Icarus* **14**, 59-70.

Wasson J. T. and Wang J. (1986) A nonmagmatic origin of group IIE iron meteorites. *Geochim. Cosmochim. Acta* **50**, 725-732.

Wasson J. T., Willis J., Wai C. M., and A K. (1980) Origin of iron meteorite groups IAB and IIICD. *Zeits. Naturforsch.* **35a**, 781-795.

Wasson J. T., Ouyang X., Wang J., and Jerde E. (1989) Chemical classification of iron meteorites: XI. Multi-element studies of 38 new irons and the high abundance of ungrouped irons from Antarctica. *Geochim. Cosmochim. Acta* **53**, 735-744.

Weigel A., Eugster O., Koeberl C. and Krähenbühl U. (1994) The Iodranite class: Asteroid break-up and chemical composition (abstract). *Meteoritics* **29**, 548.

Weisberg M. K., Prinz M., and Nehru C. E. (1988) Petrology of ALH85085: A chondrite with unique characteristics. *Earth Planet. Sci. Lett.* **91**, 19-32.

Weisberg M. K., Prinz M., Clayton R. N., and Mayeda T. K. (1993) The CR (Renazzo-type) carbonaceous chondrite group and its implications. *Geochim. Cosmochim. Acta* **57**, 1567-1586.

Widom E., Rubin A. E., and Wasson J. T. (1986) Composition and formation of metal nodules and veins in ordinary chondrules. *Geochim. Cosmochim. Acta* **50**, 1989-1995.

Wlotzka F. (1993) A weathering scale for the ordinary chondrites (abstract). *Meteoritics* **28**, 460.

Yanai K. and Kojima H. (1995) Yamato-8451: A newly identified pyroxene-bearing pallasite. *Proc. NIPR Symp. Ant. Met.* **8**, 1-10.

Zipfel J. and Palme H. (1993) Chemical composition of new acapulcoites and Iodranites (abstract). *Lunar Planet. Sci.* **24**, 1579-1580.

Table 1. Metal compositions of NWA 468 and GRV 98003 obtained by INAA.

meteorite	Cr	Co	Ni	Cu	Ga	Ge	As	Sb	W	Re	Ir	Pt	Au
	µg/g	mg/g	mg/g	µg/g	µg/g	µg/g	µg/g	ng/g	µg/g	ng/g	µg/g	µg/g	µg/g
NWA 468	4505	7.22	119.2	282	31.3	124	22.9	421	0.62	292	2.80	4	2.253
NWA 468	45	7.16	117.8	243	30.6	109	22.7	441	0.67	270	2.70	3.9	2.174
NWA 468 mean	2300	7.19	118.5	263	31.0	117	22.8	431	0.65	281	2.75	4.0	2.214
Grove Mountains 98003	12	6.89	146.3	371	6.96	<50	22.0	404	0.60	<40	0.068	5.9	2.158

The samples also contain major amounts of Fe which can be determined by difference.

Table 2. Mean composition of the silicate portion of NWA 468 and bulk MAC 88177 determined by INAA.

lithophile elements		
	NWA 468	MAC 88177
Al (mg/g)	3.2	2.4
Sc (µg/g)	20.6	9.27
Ca (mg/g)	36.0	9.85
La (ng/g)	118	104
Sm (ng/g)	35	66
Eu (ng/g)	11	12
Yb (ng/g)	97.0	148
Lu (ng/g)	20	26
V (µg/g)	398	96.7
Mg (mg/g)	187	221
Cr (mg/g)	27.5	4.42
Mn (mg/g)	3.16	3.52
Na (mg/g)	0.74	0.36
K (µg/g)	15	17
siderophile and chalcophile elements		
Ir (ng/g)	13	30
Ru (ng/g)	94.0	130
Ni (mg/g)	1.8	3.5
Co (µg/g)	85.0	137
Fe (mg/g)	134	136
Au (ng/g)	21	34
As (µg/g)	0.21	0.33
Cu (µg/g)	81	56
Ga (µg/g)	1.3	2.6
Sb (ng/g)	24	41
Se (µg/g)	14.3	6.66
Zn (µg/g)	48	64

The MAC 88177 data are from a previously unpublished analysis at UCLA.

Table 3. Modal abundances of two silicate clasts in NWA 468 and of the MAC 88177 whole rock.

	clast A		clast B		MAC 88177	
mineral	vol.%	wt.%	vol.%	wt.%	vol.%	wt.%
silicate			92.7	90.0	93.6	90.3
olivine	34.9	32.2				
low-Ca cpx	10.9	10.0				
low-Ca opx	26.8	24.8				
diopside	11.6	10.8				
plagioclase	1.8	1.3				
chromite	2.3	3.0	1.0	1.4	0.8	1.1
troilite	6.0	7.9	5.8	8.0	3.3	4.5
metallic Fe-Ni			<0.1	<0.1	1.2	2.7
kamacite	1.7	3.8				
plessite	1.1	2.5				
taenite	0.1	0.2				
schreibersite	0.1	0.2				
limonite	2.7	3.3	0.5	0.6	1.2	1.4
total	100.0	100.0	100.0	100.0	100.1	100.0
no. of points	1900		1327		1483	
area (mm^2)	98		45		60	

Phases in clast A were measured microscopically using thin section LC 931; modal abundances of individual silicate minerals were measured with the electron microprobe. The two modes were combined. Phosphate was searched for but not found. Clast B was measured in reflected light with slab LC 1706. MAC 88177,16 was measured in thin section. Weight percent was calculated from vol.% using the following mineral specific gravities: bulk silicate, 3.3; olivine, 3.28; low-Ca clinopyroxene (cpx) and low-Ca orthopyroxene (opx), 3.28; diopside, 3.3; plagioclase, 2.65; chromite, 4.7; troilite, 4.67; bulk metallic Fe-Ni, 7.95; kamacite, 7.85; plessite, 7.95; taenite, 8.19; schreibersite, 7.2; limonite, 4.28. The specific gravities of olivine, low-Ca pyroxene and plagioclase are based on the mean compositions of these phases in clast A.

Table 4. Mean compositions (wt.%) of major phases in NWA 468.

	olivine	low-Ca pyx	Ca-pyx	plagioclase	chromite (fine)	chromite (coarse)
no. of grains	10	6	2	14	8	5
SiO_2	41.0±0.3	57.0±0.3	53.8±0.5	64.4±0.9	0.20±0.16	<0.04
TiO_2					0.35±0.08	0.43±0.19
Al_2O_3	<0.04	0.27±0.03	0.64±0.04	22.7±0.7	6.9±1.2	6.9±1.0
Cr_2O_3	0.10±0.03	0.41±0.03	1.0±0.1		61.7±1.3	64.8±1.5
FeO	5.2±1.2	6.0±0.2	2.3±0.1	0.40±0.37	16.4±0.8	12.0±1.0
MnO	0.39±0.06	0.48±0.07	0.31±0.11		0.95±0.07	1.2±0.1
MgO	52.1±0.9	33.8±0.4	17.6±0.0		10.1±0.3	12.6±0.7
CaO	0.05±0.04	0.99±0.06	21.9±0.6	3.9±0.5	0.28±0.21	<0.04
Na_2O				9.0±0.2		
K_2O				0.45±0.14		
total	98.8	99.1	97.6	100.9	97.0	97.9
endmember	$Fa_{5.3±1.2}$	$Fs_{8.9±0.3}$ $Wo_{1.9±0.1}$	$Fs_{3.7± 0.1}$ $Wo_{45.4±0.7}$	$Ab_{78.7±1.7}$ $Or_{2.6±0.9}$		

	kamacite	taenite	troilite	schreibersite
no. of grains	10	8	7	7
Fe	91.6±0.7	76.1±6.5	61.2±0.7	47.9±6.7
Ni	7.2±0.2	22.9±6.5	<0.05	33.5±6.7
Co	0.62±0.04	0.15±0.09	<0.05	<0.05
P	n.d.	n.d.	n.d.	18.5
S	<0.05	<0.05	37.2±0.5	0.08±0.02
Cr	<0.05	<0.05	0.75±0.21	<0.05
total	99.4	99.2	99.2	100.0

Fine chromite grains are typically <20 μm in size; coarse chromite grains are generally 100-300 μm. Low-Ca pyx analyses include both orthorhombic and monoclinic grains. n.d. = not determined. P in schreibersite determined by difference.

Figure Captions

Fig. 1. Element-to-Au diagrams of the metal composition that show the relationship between NWA 468 and the other members of the IAB complex. The main group (MG) is represented by the dense cluster of dark diamonds at the left-hand side of each diagram. The subgroups (e.g., sLH) show fractionation trends similar to those in the main group. NWA 468 (NWA), represented by a gray triangle, does not belong to the main group or the subgroups, but is compositionally related to Grove Mountains 98003 (GRV) (another gray triangle) and, to a lesser degree, sHL Lonaconing (Lon) and Ventura (Ven), and ungrouped Sombrerete (Som), Yamato 8451 (Y84) and Vermillion (Ver). sLH = low-Au, high-Ni subgroup (dark filled circles); sHL = high-Au, low-Ni subgroup (gray squares); sHH = high-Au, high-Ni subgroup (gray circles); sLL = low-Au, low-Ni subgroup (x's).

Fig. 2. Elemental abundances of the mean composition of two metal replicates of NWA 468 normalized to Ni and to CI carbonaceous chondrites. Refractory and volatile siderophiles are depleted relative to Ni, Co, Au and As. Also shown are the elemental abundances of GRV 98003; this meteorite has a similar abundance pattern for Pt, Ni, Co, Fe, Au, As and Cu, but has lower Re, Ir, Ga, Ge and Cr abundances than NWA 468. Elements are plotted from left to right in order of increasing volatility (except for mainly oxyphile Cr which has a volatility similar to that of Fe and is plotted on the far right).

Fig. 3. The bulk composition of silicate in NWA 468 and whole rock composition of the lodranite MAC 88177 normalized to Mg and to CI carbonaceous chondrites; elements are divided into two groups: lithophiles on the left, siderophiles, chalcophiles and Zn on the right. (Although Zn is plotted next to Se, it is possible that Zn is mainly lithophile in these meteorites.) Within each group, the elements are plotted from left to right in order of increasing volatility. Both meteorites show typical lodranite lithophile patterns consisting of low Al, higher Sc and Ca, fractionated REE with negative Eu anomalies, and depleted Na and K (cf. Fig. 4). The high V and Cr abundances in NWA 468 probably reflect a substantial chromite enhancement in our silicate sample; the high Fe, Cu and Se probably reflect significant amounts of troilite. The main differences in the silicate abundance patterns of NWA 468 and MAC 88177 are in the much lower abundances of V and Cr and the smaller Se peak in MAC 88177.

Fig. 4. The bulk compositions of the silicate portions of lodranites normalized to Mg and to CI carbonaceous chondrites. The lithophile pattern of MAC 88177 is representative of lodranites. MAC 88177 was analyzed at UCLA; data for the other lodranites are from the literature: Haramura et al. (1983), Nagahara and Ozawa (1986), Torigoye et al. (1993), Weigel et al. (1994) and Dreibus et al. (1995).

Fig. 5. Standard oxygen-isotope diagram showing the composition of NWA 468 silicate compared to that of other meteoritic objects. It lies outside the main IAB field but close to CH and CR carbonaceous chondrites, lodranites, acapulcoites and several ungrouped irons including Sombrerete, Vermillion and Y8451. (The latter two were called pallasite-an by Clayton and Mayeda, 1996). All data are from Clayton and Mayeda (1996) and other publications from R. N. Clayton's laboratory.

Fig. 6. Whole-rock specimen of NWA 468 showing massive silicates (black) and metal (white). This 22-cm^2 slab (LC 1706) from the UCLA meteorite collection contains ~55 vol.% silicate and ~45 vol.% metallic Fe-Ni. Silicate clast B is the 1.5-cm-long dark object just to the left of center. The light-gray halo around the clast is caused by the enrichment of troilite near the clast margins. Scale bar is in centimeters.

Fig. 7. Textures within the silicate clasts. (a) Spidery network of troilite (tr; light gray near center) near the margins of silicate clast B. Silicate (sil; dark gray); metal (met; white). Reflected light. (b) Coarse polysynthetically twinned low-Ca clinopyroxene grain in silicate clast A. Crossed nicols. (c) Troilite (tr; light gray) with multiple appendages amidst silicate (dark gray) in clast A. The light gray phase within the troilite is a terrestrial weathering product. Reflected light. (d) Clouds of small wormy troilite particles (very light gray) adjacent to chromite (chr; light gray) and coarse troilite partially weathered to limonite (lim; medium gray). Silicate = sil. Surrounding silicate (dark gray). Reflected light.

Fig. 8. Metallic Fe-Ni textures. (a) Fields of duplex plessite located several millimeters away from the silicate clasts. Sparks and spindles of kamacite (light gray) are surrounded by fine-grained plessitic regions (pl; dark gray); many of the kamacite grains have resolvable schreibersite patches (sch; medium gray) in their centers. Reflected light. (b) Shafts of schreibersite (sch; light gray, running ENE-WSW across the image) rimmed by swathing kamacite (kam; very light gray). These shafts occur between the large fields of duplex plessite (pl; dark gray). Plucked areas and limonite (both black) occur along the schreibersite shaft. Reflected light.

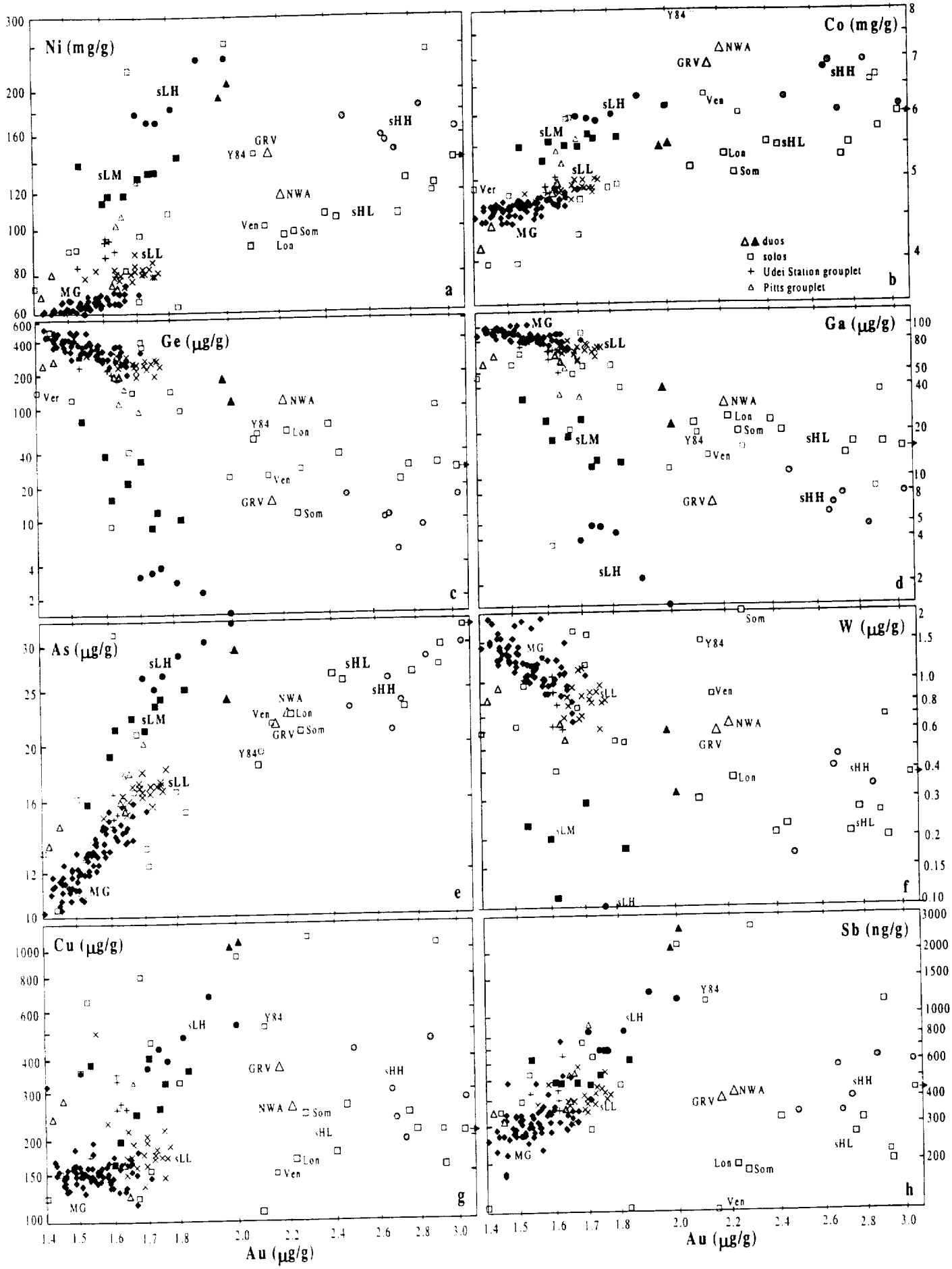
Ni (mg/g)
Co (mg/g)
Ge (μg/g)
Ga (μg/g)
As (μg/g)
W (μg/g)
Cu (μg/g)
Sb (ng/g)
Au (μg/g)
Au (μg/g)
sLH
sLM
sLL
sHH
sHL
GRV
NWA
Y84
Ven
Lon
Som
MG
Ver
duos
solos
Udei Station grouplet
Pitts grouplet
a
b
c
d
e
f
g
h

Fig. 1

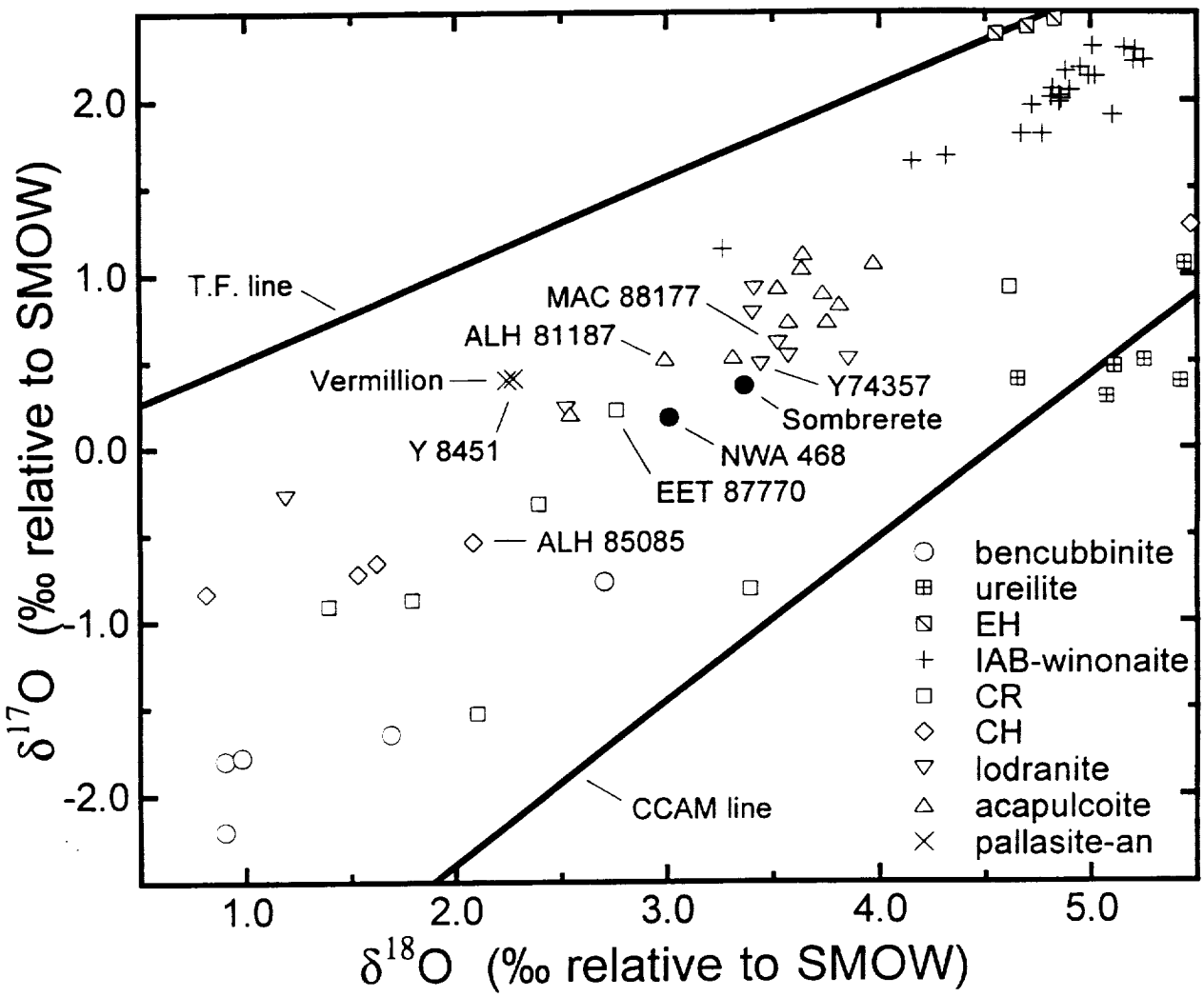
2.0
1.0
0.0
-1.0
-2.0
1.0
2.0
3.0
4.0
5.0
δ17O (‰ relative to SMOW)
δ18O (‰ relative to SMOW)
T.F. line
CCAM line
MAC 88177
ALH 81187
Vermillion
Y 8451
Y74357
Sombrerete
NWA 468
EET 87770
ALH 85085
bencubbinite
ureilite
EH
IAB-winonaite
CR
CH
lodranite
acapulcoite
pallasite-an

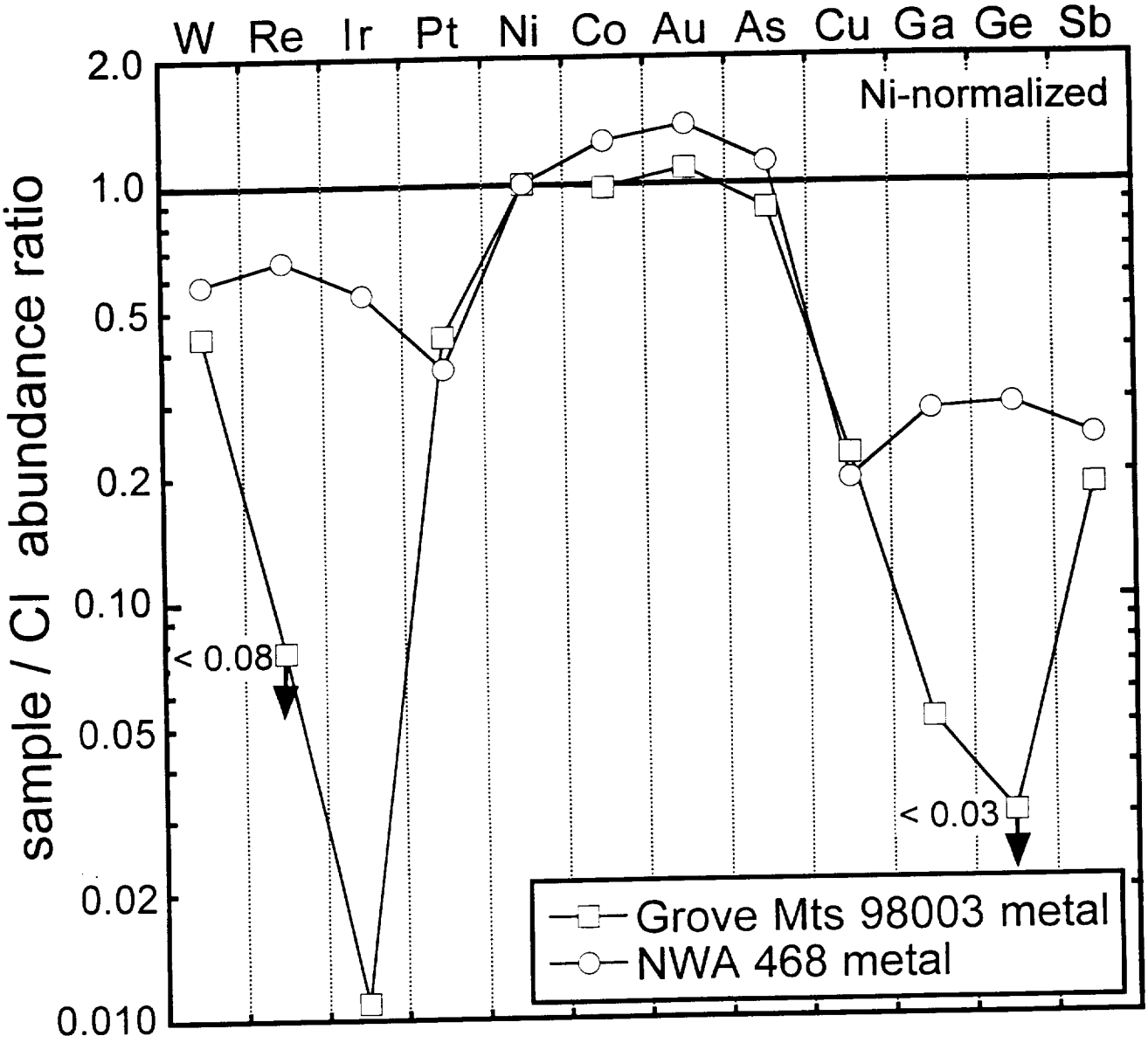
W Re Ir Pt Ni Co Au As Cu Ga Ge Sb
2.0
1.0
0.5
0.2
0.10
0.05
0.02
0.010
sample / CI abundance ratio
Ni-normalized
< 0.08
< 0.03
Grove Mts 98003 metal
NWA 468 metal

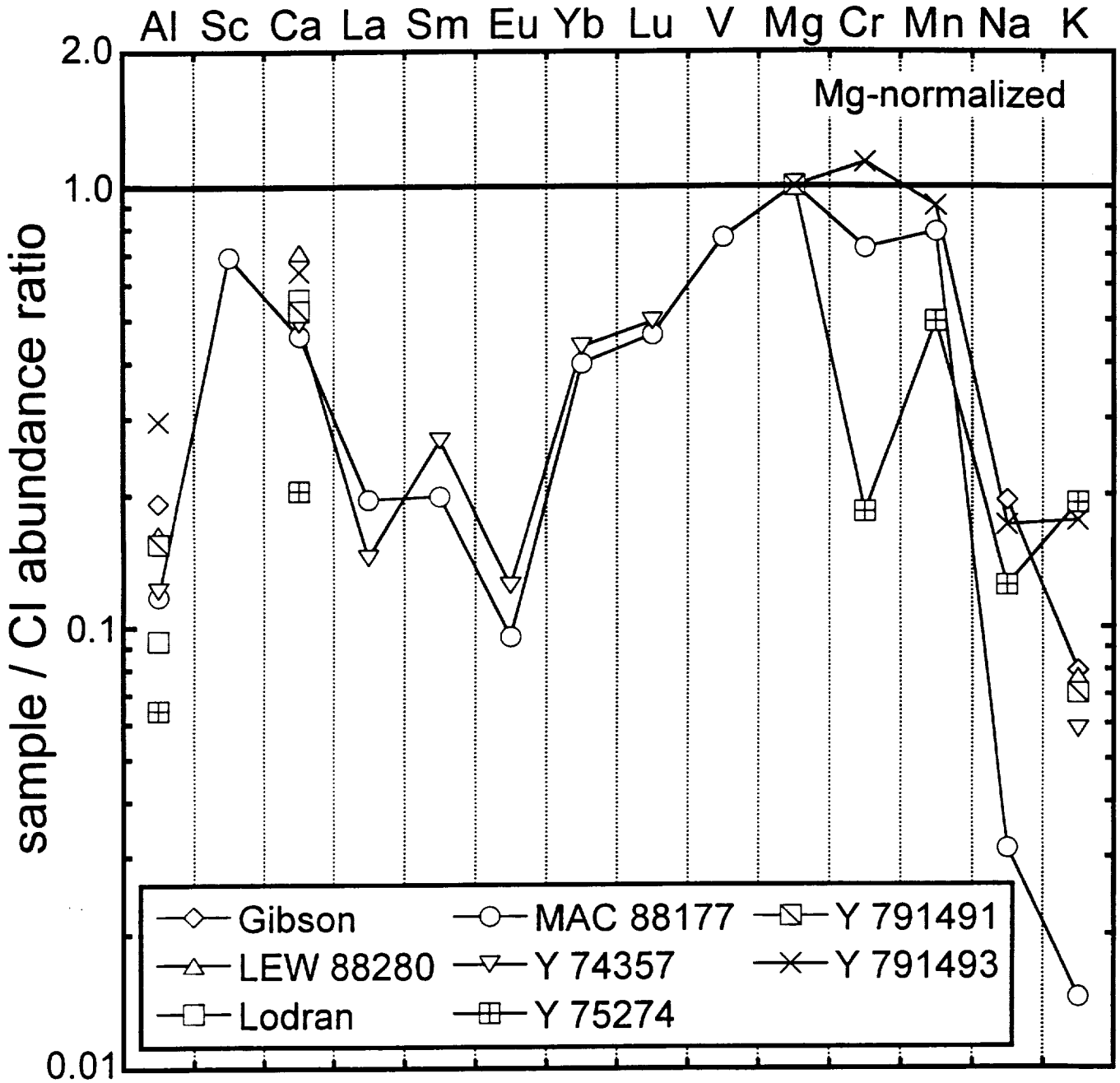
Al Sc Ca La Sm Eu Yb Lu V Mg Cr Mn Na K
2.0
1.0
0.1
0.01
Mg-normalized
sample / CI abundance ratio
Gibson
MAC 88177
Y 791491
LEW 88280
Y 74357
Y 791493
Lodran
Y 75274

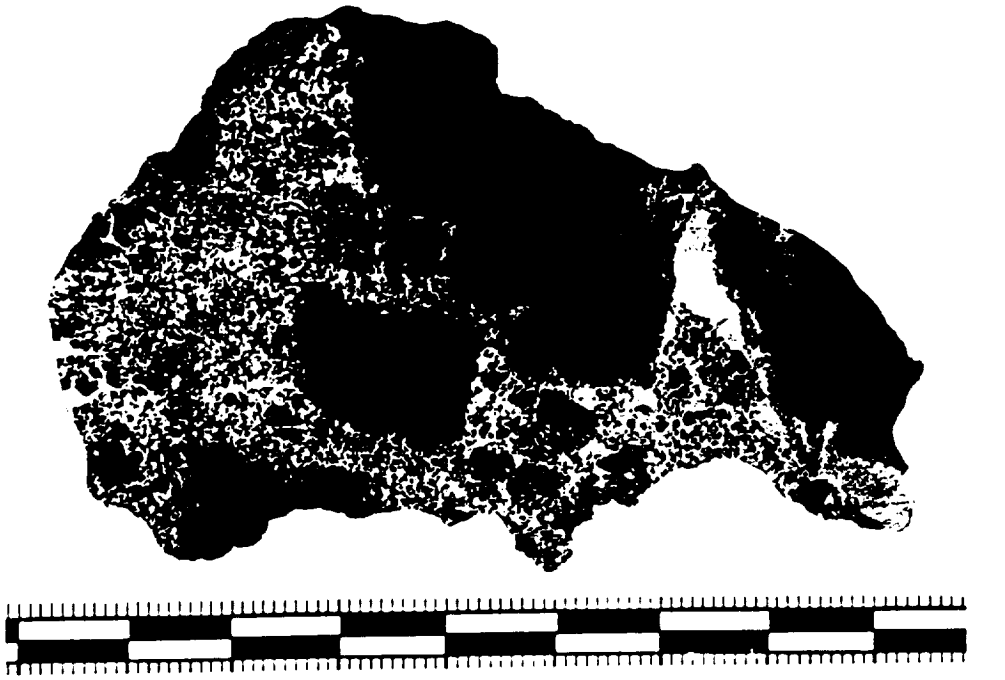

Fig.6

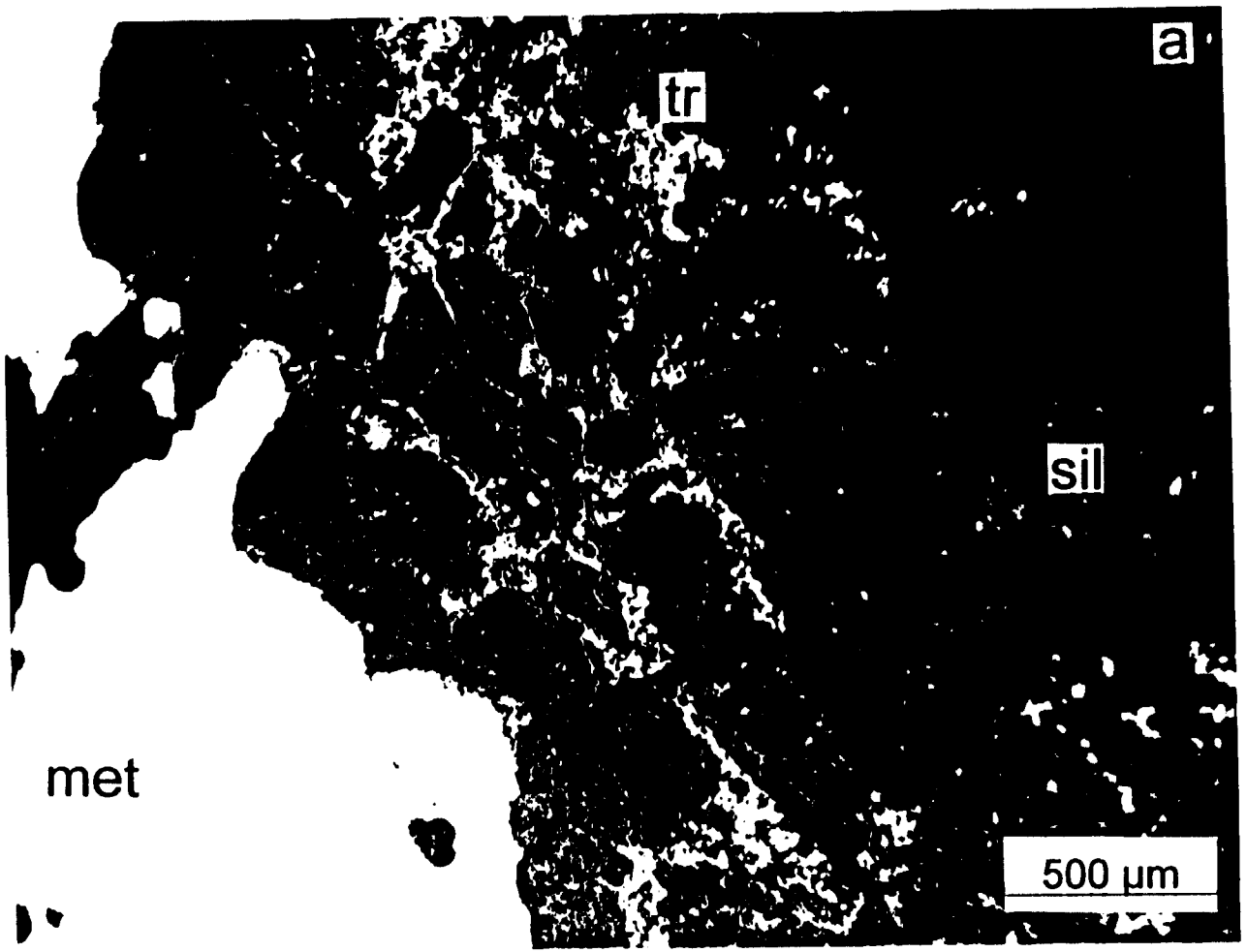

Fig. 7a

Fig. 7b

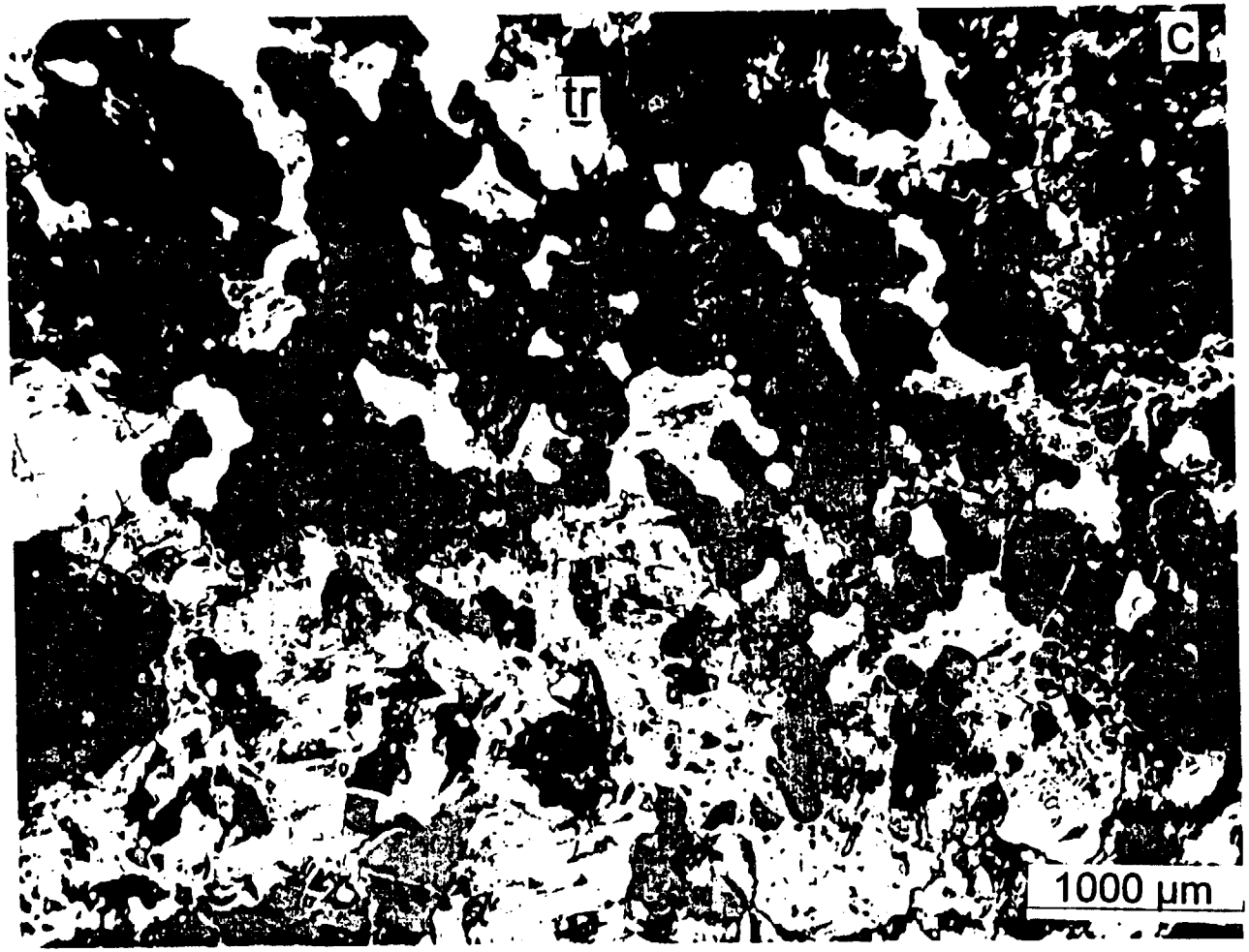

Fig. 7c

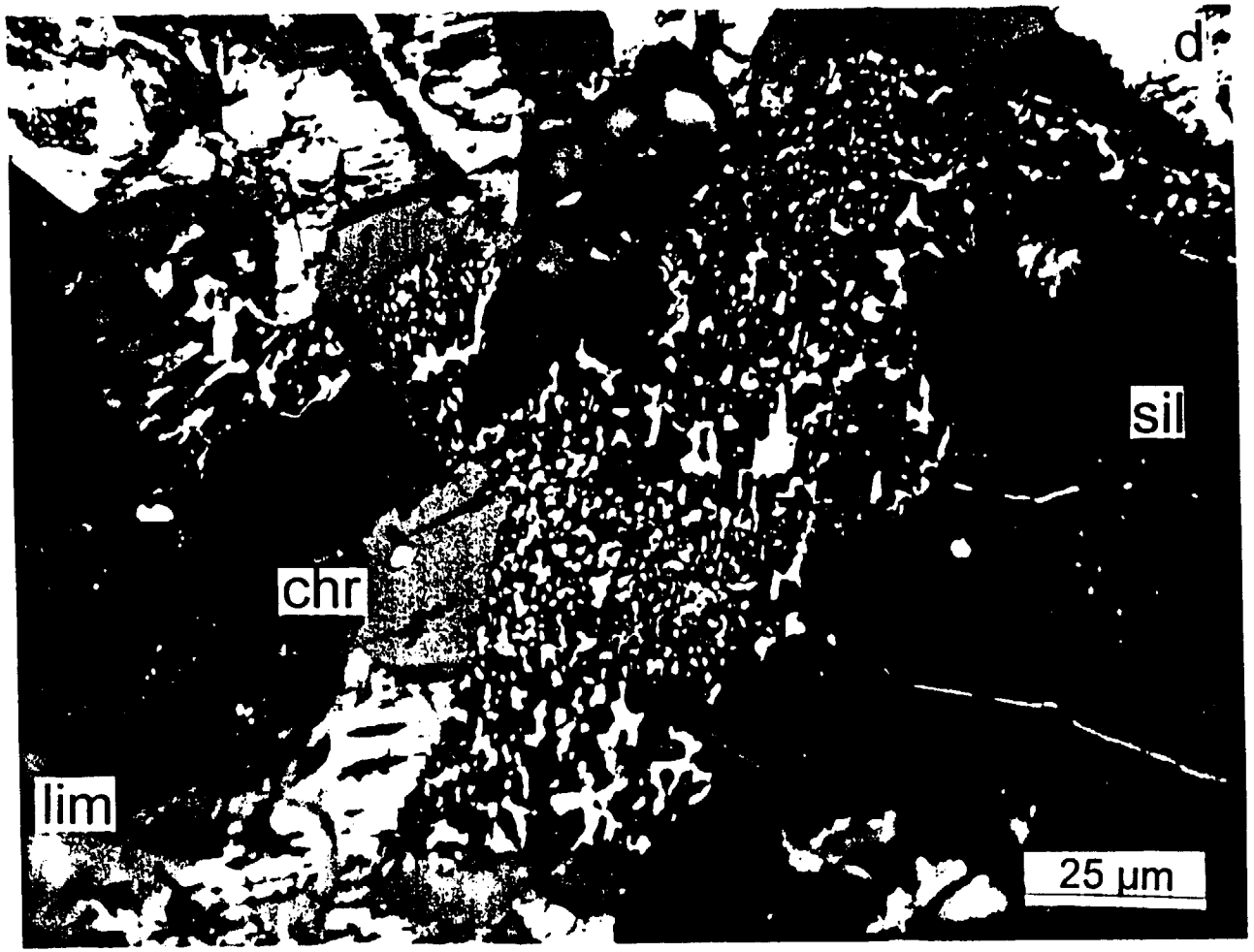

Fig. 7d

Fig. 8a

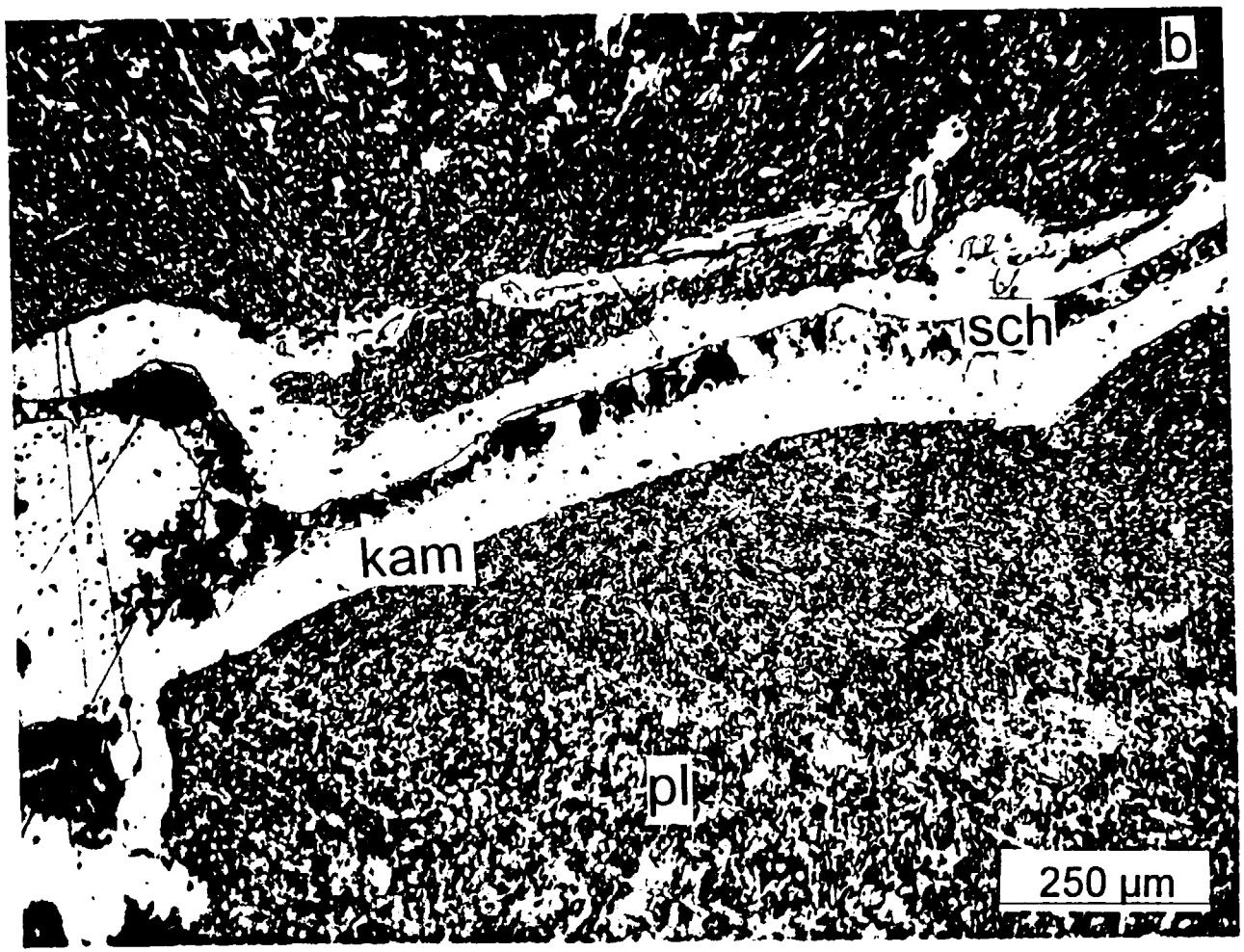

Fig. 8b